Lindblad and Redfield Master Equations for Predicting Crosstalk-Induced Decoherence on IBM Quantum Devices

Luke Lopez, Rodrigo Lopez, Dhruv 'Bala' Balasubramanian

May 2025

Abstract

In this study, we investigate crosstalk-induced decoherence on IBM Sherbrooke by employing both Lindblad and Bloch-Redfield master equations. Our experimental setup features a three-qubit system comprising one target qubit and two directly coupled spectator qubits, with empirically determined coupling strengths. The Lindblad formulation assumes Markovian dynamics, while the Bloch-Redfield approach incorporates non-Markovian behavior through weak coupling to an Ohmic bath. We examine the decay dynamics of the target qubit's $|1\rangle$ state population when the spectator qubits are prepared in three different states: $|1\rangle$, $|0\rangle$, and $|+\rangle$. These theoretical predictions are validated against experimental measurements on qubits 100,110,118. Both theoretical frameworks predict faster population decay than observed experimentally. Notably, the Bloch-Redfield equation severely underestimates crosstalk impacts. Experimental observations reveal that decay rates are minimized when spectator qubits are in the $|+\rangle$ state; however, numerical instabilities prevent the Redfield equation from accurately simulating this configuration. Neither theoretical model fully captures the experimental behavior.

1 Background

1.1 Crosstalk

Crosstalk describes unintended interactions between adjacent qubits that can influence a qubit's quantum state. Such interactions contribute to unwanted decoherence, resulting in computational errors and reduced measurement fidelity. Understanding and controlling crosstalk is crucial for enhancing the performance and reliability of quantum algorithms on near-term quantum devices.

1.2 Prior Work

Prior studies have addressed crosstalk mitigation through hardware and software methods. IBM researchers suggested a technique called dynamic instruction reordering to minimize simultaneous activation of coupled qubits, using scheduling to suppress crosstalk instead of hardware changes [1]. Other techniques, like dynamical decoupling, have been introduced to handle ZZ-type crosstalk in superconducting systems [2].

For modeling, the Lindblad master equation is popular for noise simulation on NISQ devices due to its simplicity and complete positivity. However, it has limitations in capturing time-correlated errors and environmental memory effects [3]. The Bloch-Redfield formalism can provide more accurate descriptions for systems with structured environments or low-frequency noise, although it is less commonly applied in practice [4].

There is a lack of side-by-side comparisons between Lindblad and Redfield predictions using real quantum hardware data. Most experiments either rely on idealized decoherence models or address crosstalk phenomenologically without linking it to a first-principles Hamiltonian. This study aims to bridge that gap.

2 Methods

At a high level, we model crosstalk between directly connected qubits on the IBM Sherbrooke device. We consider one configuration where qubit 110 is the target, and qubits 100 and 118 are spectators. Refer to Figure 1 for an illustration. Using Lindblad and Bloch-Redfield master equations, we simulate the time evolution of the full three-qubit system and predict the population decay of the target qubit's $|1\rangle$ population. These predictions are compared to delayed measurements on IBM hardware.

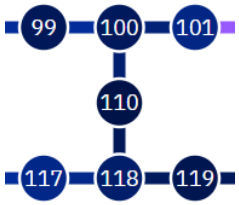

Figure 1: Experimental Coupling Map

2.1 Model Assumptions

As stated above, in this study, our quantum simulations employ two complementary approaches to model three coupled superconducting qubits. We experi-

mented with several different theoretical assumptions and modeling approaches, ultimately settling on these particular formulations due to their optimal balance between accuracy in reproducing our observed experimental data and numerical solvability. We use a simplified Lindblad model and a more comprehensive Bloch-Redfield model, testing different approximation levels while keeping our extracted qubit parameters to identify which theoretical framework most accurately reproduces the observed quantum dynamics while remaining computationally tractable. Both models assume constant coupling strengths between qubits. The coupling architecture follows a linear chain topology where qubit 110 serves as the target qubit connecting spectator qubits 100 and 118, with no direct interaction between the end qubits, matching IBM's typical nearest-neighbor connectivity pattern. After exploring more complex coupling schemes, we found this simplified topology provided the best compromise between modeling accuracy and computational efficiency.

Both models treat qubit frequencies and detunings differently, with our final choice based on extensive comparison with experimental data. The Lindblad approach completely neglects individual qubit frequencies and their associated detunings as a limiting case, while the Bloch-Redfield model includes them but assumes the large frequency differences justify the rotating wave approximation (RWA). We initially tested models with full frequency dependence and various levels of approximation, but found that the rotating wave approximation provided the best fit to our data while maintaining numerical stability. By comparing these approaches, we assess whether the significant energy differences between qubits must be explicitly included to achieve accurate modeling of the experimental system dynamics. The decoherence models assume different noise characteristics, chosen after evaluating multiple noise models against our experimental observations: the Lindblad approach assumes purely Markovian dynamics with white noise and no memory effects, while the Bloch-Redfield model incorporates non-Markovian behavior through frequency-dependent spectral densities that allow for environmental memory effects. Both approaches treat T_1 decay and T_2 dephasing according to standard relationships, with the Bloch-Redfield model explicitly modeling frequency-structured noise.

This comparison allows us to determine whether the additional complexity of the Bloch-Redfield model provides significantly better agreement with experimental data.

We assume ideal state preparation for all computational states without accounting for state preparation errors, allowing us to focus on the evolution dynamics rather than initialization imperfections. Both models track expectation values or populations directly without modeling the probabilistic nature of quantum measurements, treating the measurement process as ideal projective measurements. All system parameters including coherence times and coupling strengths are assumed time-independent, neglecting potential drift or temporal variations observed in quantum hardware.

These simplifications enable us to isolate the essential physics of qubit cou-

pling and decoherence while maintaining computational tractability for parameter fitting. The theoretical frameworks employ the rotating wave approximation through exchange-type interactions. While the Lindblad model assumes strictly Markovian environmental dynamics, the Bloch-Redfield model can capture non-Markovian effects through its frequency-dependent spectral densities. However, both simulations neglect control imperfections, gate errors, crosstalk beyond nearest neighbors, and complex environmental correlations that would be present in real quantum systems. The choice of which approximations to include was guided by extensive testing and comparison with experimental results, where we systematically added and removed various effects to determine the minimal model complexity required to achieve satisfactory agreement with our observations.

All qubit parameters (T_1, T_2, and frequency) were directly extracted from IBM Sherbrooke using Qiskit's backend function. The coupling strengths J were empirically determined, with the coupling between qubits 100-110 assumed to be equal to the coupling between qubits 110-118. We also assume that ZZ coupling is equal to XX coupling in our model, providing a simplified but consistent representation of the inter-qubit interactions.

Qubit	T1 (s)	T2 (s)	Frequency (Hz)
110.0	0.0001793571394	0.0002101960696	4834494948.0
100.0	0.0003217494089	0.0004053855277	4648611297.0
118.0	0.0002229329027	0.0003185100771	4737492574.0

Figure 2: IBM Sherbrooke Qubit Parameters

2.2 Lindblad Model

The density matrix ρ evolves according to:

$$\frac{d\rho}{dt} = -i[H, \rho] + \sum_k \left(L_k \rho L_k^\dagger - \frac{1}{2}\{L_k^\dagger L_k, \rho\} \right)$$

Here, ρ is the full three-qubit density matrix (target and spectators).

In the Lindblad simulation, the Hamiltonian is constructed without individual qubit frequencies (RWA), implementing only exchange coupling between adjacent qubits:

$$H = J(\sigma^x_{110} \otimes \sigma^x_{100} + \sigma^y_{110} \otimes \sigma^y_{100}) + J(\sigma^x_{110} \otimes \sigma^x_{118} + \sigma^y_{110} \otimes \sigma^y_{118})$$

J, the coupling strength coefficient, is derived empirically. For simplicity, we assume a uniform coupling strength between the XX and YY terms. For details on deriving J, see section 2.4.

As stated above, this simplified approach neglects the individual qubit energies $\frac{\hbar\omega_i}{2}\sigma_i^z$and their detunings, focusing solely on the energy exchange between qubits mediated by the XX + YY interaction terms, which correspond to the rotating wave approximation of the exchange interaction.

We assume independent amplitude damping and pure dephasing on each qubit. Lindblad operators are constructed using T_1 and T_2 values from IBM calibration data:

$$\gamma_1^{(i)} = \frac{1}{T_1^{(i)}}, \quad \gamma_\phi^{(i)} = \max\left(0, \frac{1}{T_2^{(i)}} - \frac{1}{2T_1^{(i)}}\right)$$

All six Lindblad operators used are:

$$\begin{aligned}
L_{T1,i} &= \sqrt{\gamma_1^{(i)}}\sigma^- \otimes I \otimes I \\
L_{T1,j} &= \sqrt{\gamma_1^{(j)}} I \otimes \sigma^- \otimes I \\
L_{T1,k} &= \sqrt{\gamma_1^{(k)}} I \otimes I \otimes \sigma^- \\
L_{\phi,i} &= \sqrt{\gamma_\phi^{(i)}}\sigma_z \otimes I \otimes I \\
L_{\phi,j} &= \sqrt{\gamma_\phi^{(j)}} I \otimes \sigma_z \otimes I \\
L_{\phi,k} &= \sqrt{\gamma_\phi^{(k)}} I \otimes I \otimes \sigma_z
\end{aligned}$$

where i, j, k represent the qubits 100, 110 and 118 respectively.

Simulations are performed with `qutip.mesolve`. We track the $|1\rangle$ amplitude of the target qubit over time and compare the results to hardware measurements. In practice, we would take the partial trace over our spectator qubits for the density matrix ρ, but QuTiP conveniently handles this for us, allowing us to directly monitor the target qubit's population while properly accounting for the full system dynamics.

2.3 Bloch-Redfield Model

For our Redfield Model, we assume the Hamiltonian type to be transverse Ising Hamiltonian.

$$H = H_{individual} + H_{coupling}$$

Where,

$$H_{individual} = -\frac{1}{2}\omega_{100}\sigma_z^{(100)} \otimes I \otimes I - \frac{1}{2}\omega_{110} I \otimes \sigma_z^{(110)} \otimes I - \frac{1}{2}\omega_{118} I \otimes I \otimes \sigma_z^{(118)}$$

and,

$$H_{coupling} = J\left(\sigma_x^{(100)} \otimes \sigma_x^{(110)} \otimes I + \sigma_y^{(100)} \otimes \sigma_y^{(110)} \otimes I\right) + J\left(I \otimes \sigma_x^{(110)} \otimes \sigma_x^{(118)} + I \otimes \sigma_y^{(110)} \otimes \sigma_y^{(118)}\right)$$

where again, J is assumed uniform across XX and YY terms and is derived empirically from the process described in 2.4.

The Redfield master equation takes the form:

$$\frac{d\rho}{dt} = -i[H, \rho] - \sum_{\omega,\omega'} \sum_{\alpha,\beta} \left(R_{\alpha\beta}(\omega, \omega') \left[A_\alpha^\dagger(\omega'), A_\beta(\omega)\rho\right] + \text{H.c.}\right)$$

where $R_{\alpha\beta}(\omega, \omega')$ is the Redfield tensor computed from the spectral density of the noise, and $A_\alpha(\omega)$ are transition operators in the eigenbasis of H. The derivation follows the standard formalism described in Lidar, Ch. 13.2–13.3 [3].

We assume each qubit is independently coupled to an Ohmic environment with the spectral density:

$$J(\omega) = \eta\, \omega\, \Theta(\omega)$$

where η is a dimensionless coupling constant derived from experimental T_1 and T_2 values, and $\Theta(\omega)$ is the Heaviside step function enforcing positivity of frequency.

This noise model is implemented using `qutip.BlochRedfieldTensor`, which internally diagonalizes the system Hamiltonian, computes all Bohr frequencies ω, and evaluates the Redfield tensor components based on the assumed spectral density. Time evolution is performed using `qutip.brmesolve`, and the target qubit's excited-state population is extracted at each time step by tracing over the spectator qubits.

2.4 Derivation of Coupling Strength Coefficient (J)

To accurately model our system, we employ free evolution experiments to extract the coupling parameter J between our target qubit and its spectator qubits. This coupling represents a key source of crosstalk in superconducting quantum processors, causing unwanted interactions even when no explicit operations connect the qubits.

The physical basis for this extraction lies in the system Hamiltonian with ZZ-type interactions:

$$H = \Omega Z_t \otimes I_s + J(Z_t \otimes Z_{s1} + Z_t \otimes Z_{s2})$$

where Ω represents the qubit frequency, Z_t is the Pauli-Z operator on the target qubit, and Z_{s1}, Z_{s2} are Pauli-Z operators on the spectator qubits. The coupling strength J is precisely the parameter we aim to extract.

Using the circuit shown below in Figure 3, we extract ZZ coupling parameters through free evolution experiments on the target qubit. The Hadamard (H) gates create a superposition state ($|+\rangle$) on the target qubit while the spectator qubits are initialized in either $|0\rangle$ or $|1\rangle$ states, resulting in initial system states of $|0+0\rangle$ or $|1+1\rangle$ respectively. During the subsequent free evolution period, ZZ interactions between the target and spectators cause state-dependent phase accumulation, with the interaction strength differing between the two configurations.

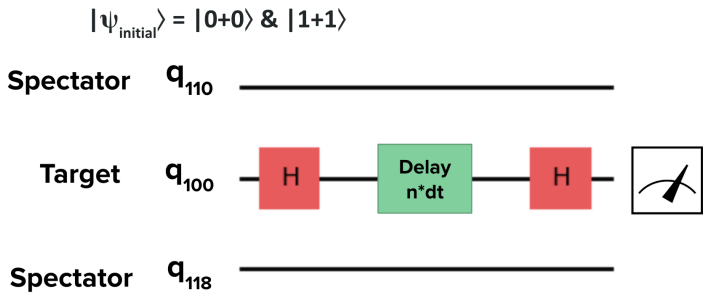

Figure 3: Coupling Extraction Circuit

When we prepare the target qubit in $|+\rangle$ state and spectators in state $|0\rangle$ or $|1\rangle$, the system evolution follows distinct patterns. Theoretically, the target qubit fidelity for these two configurations follows:

$$F_{+0}(t) = \frac{1}{2}[1 + \cos(2(\Omega + J)t)]$$

$$F_{+1}(t) = \frac{1}{2}[1 + \cos(2(\Omega - J)t)]$$

The difference in oscillation frequencies arises because the ZZ coupling effectively shifts the target qubit frequency depending on the state of the spectator qubits. When spectators are in $|0\rangle$, the target experiences a frequency shift of $+J$, while spectators in $|1\rangle$ cause a shift of $-J$.

By analyzing the target qubit's fidelity as a function of spectator state configurations and evolution times, we extract the coupling strength from variations

in oscillation frequencies. The collected experimental data, shown in Figure 4 below, is fitted to a damped cosine function:

$$F(t) = a + be^{-t/T_D} \cos(\omega t)$$

Here, T_D is the decoherence timescale, and ω is the oscillation frequency that reflects the effective ZZ interaction strength.

We extract two frequencies, ω_{0+0} and ω_{1+1}, corresponding to the $|0+0\rangle$ and $|1+1\rangle$ spectator states. Using the theoretical relationship between these frequencies and the coupling strength, we compute:

$$J = \frac{1}{4}(\omega_{1+1} - \omega_{0+0})$$

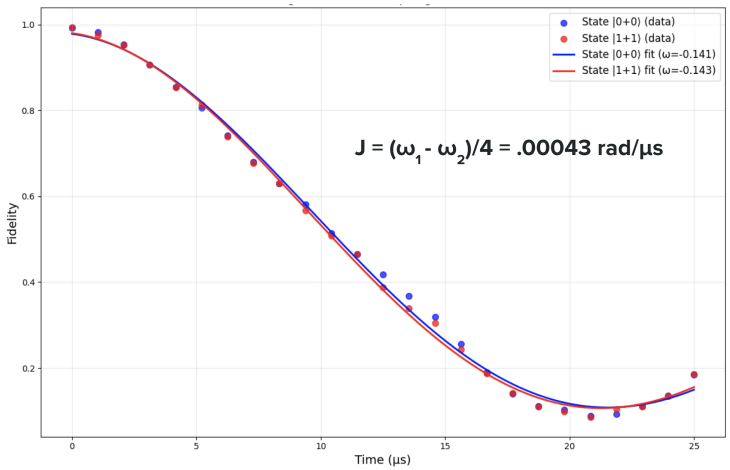

Figure 4: Coupling Extraction Data

The implementation requires precise timing control and careful circuit design. We prepare a series of circuits in the form as shown above in Figure 3, with increasing delay times between initialization and measurement, ranging from 0 to 25 μs across 25 time steps. For each delay time, we collect 3000 shots to build accurate fidelity statistics.

Fitting is performed in Python using `scipy.optimize.curve_fit`, with experiments executed and analyzed using Qiskit and Matplotlib. For our specific configuration using target qubit 110 with spectators 100 and 118 on IBM Sherbrooke, we measured:

$$\omega_{0+0} = -0.140932 \text{ rad}/\mu\text{s}, \quad \omega_{1+1} = -0.142622 \text{ rad}/\mu\text{s}$$

From these frequencies, we calculate the precise J-coupling value:

$$J = 0.0004225 \text{ rad}/\mu\text{s} \ (0.0000673 \text{ MHz})$$

Challenges in this measurement include decoherence effects that dampen the oscillations (captured by the T_D parameter) and potential systematic errors from pulse miscalibrations. The relatively small J-coupling value measured between our qubits is consistent with the improved isolation in newer generation superconducting quantum processors, but still significant enough to impact multi-qubit algorithm performance without appropriate error mitigation strategies.

3 Results

Analysis of the experimental results, displayed in Figure 5, reveals distinct decay characteristics for different neighboring qubit configurations, providing valuable insights into the coupling-induced dynamics of our three-qubit system. The data shows that the spectators $|0\rangle$ configuration exhibits the fastest qubit 110 decay, while the spectators $|1\rangle$ and $|+\rangle$ states show nearly identical, slower decay rates.

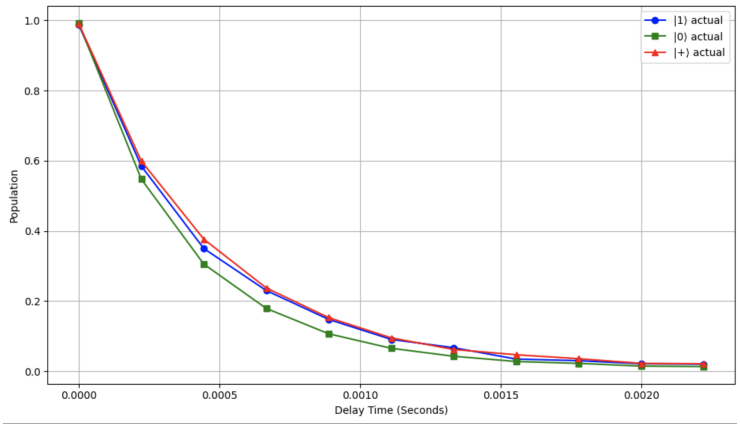

Figure 5: Experimental Data - Decay Rate of Target Qubit

The observed ordering of decay rates where $|0\rangle$ being the fastest and $|1\rangle \approx |+\rangle$ being the slowest, has important physical implications. When spectator qubits are in $|0\rangle$, they can readily accept energy from the excited central qubit 110, creating additional decay channels beyond the natural T_1 process. This enhanced energy dissipation manifests as shorter apparent T_1 times for qubit 110. Conversely, when spectators are in $|1\rangle$, they cannot accept additional excitations due to Pauli blocking, essentially reducing the available decay pathways and resulting in decay dynamics closer to the isolated qubit behavior.

The $|+\rangle$ state configuration shows interesting experimental behavior, with decay rates remarkably similar to the $|1\rangle$ case. This suggests that the super-

position nature of the $|+\rangle$ state doesn't significantly alter the energy exchange dynamics compared to fully excited neighbors. The similarity between $|1\rangle$ and $|+\rangle$ decay rates indicates that the dominant effect is the availability of empty energy levels in the spectator qubits rather than quantum interference effects between different decay pathways.

3.1 Efficacy of Model Predictions

The results summarized in Figure 6, show that across all three configurations, the experimental decay curves display slower population loss than predicted by Lindblad dynamics alone. Redfield modeling, available for the $|0\rangle$ and $|1\rangle$ cases, closely matches early-time decay when the spectators are present. However, it does not considerably outperform or underperform Lindblad, depending on the specific case. The target seems to be almost unaffected by crosstalk.

Notably, both Lindblad and Redfield predict that spectators in the $|1\rangle$ state lead to slower decoherence than spectators in the $|0\rangle$ state, aligning with experimental data. However, the Lindblad model also predicts that spectators in the $|+\rangle$ state cause faster decay than those in the $|1\rangle$ state, which contradicts the experimental observations but physically makes more sense given the smaller amount of energy present in the superposition states. Although the Redfield coupling effects are extremely small and not noticeable given the precision of the tables, they are indeed still present and contribute to the observed dynamics.

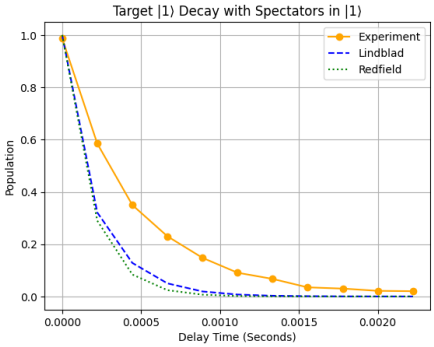

(a) Target $|1\rangle$ decay with spectators in $|1\rangle$ (graph)

Target |1⟩ Decay with Spectators in |1⟩

Time (s)	Lindblad	Redfield	Experiment
0.0	1.0	1.0	0.987
0.000222	0.321439	0.290035	0.585
0.000444	0.128458	0.08412	0.35
0.000667	0.050263	0.024262	0.230333
0.000889	0.019283	0.007037	0.148
0.001111	0.007535	0.002041	0.091
0.001333	0.002959	0.000592	0.067333
0.001556	0.001164	0.000171	0.035
0.001778	0.00046	0.000127	0.030333
0.002	0.000182	0.000127	0.021667
0.002222	0.000182	0.000127	0.020333

(b) Tabular comparison (spectators in $|1\rangle$)

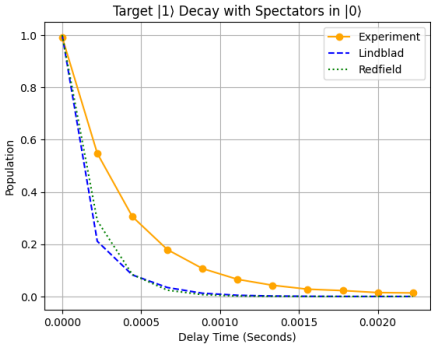

(c) Target $|1\rangle$ decay with spectators in $|0\rangle$ (graph)

Target |1⟩ Decay with Spectators in |0⟩

Time (s)	Lindblad	Redfield	Experiment
0.0	1.0	1.0	0.991667
0.000222	0.211446	0.290035	0.547667
0.000444	0.082513	0.08412	0.305667
0.000667	0.034356	0.024262	0.179333
0.000889	0.012483	0.007037	0.107
0.001111	0.004825	0.002041	0.065667
0.001333	0.0019	0.000592	0.043
0.001556	0.000743	0.000171	0.028
0.001778	0.000293	0.000127	0.022667
0.002	0.000116	0.000127	0.015
0.002222	0.000116	0.000127	0.013667

(d) Tabular comparison (spectators in $|0\rangle$)

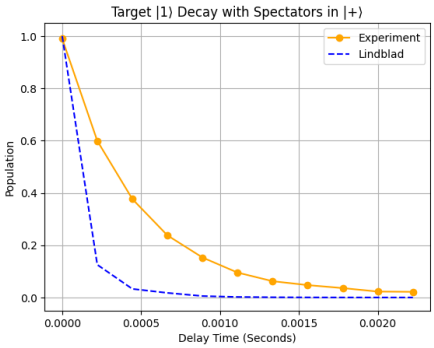

(e) Target $|1\rangle$ decay with spectators in $|+\rangle$ (graph)

Target |1⟩ Decay with Spectators in |+⟩

Time (s)	Lindblad	Experiment
0.0	1.0	0.99
0.000222	0.12538	0.599333
0.000444	0.032871	0.376667
0.000667	0.017591	0.237667
0.000889	0.005586	0.153
0.001111	0.002039	0.095333
0.001333	0.000817	0.062333
0.001556	0.000315	0.047333
0.001778	0.000123	0.036
0.002	4.9e-05	0.022667
0.002222	4.9e-05	0.021667

(f) Tabular comparison (spectators in $|+\rangle$)

Figure 6: Target qubit $|1\rangle$ decay under different spectator initializations. Each row shows the experimental decay curve (left) and the corresponding numerical comparison (right).

3.2 Limitations and Future Work

A key limitation is that our simulations assume a single uniform coupling strength J with only XX and YY terms. Another limitation is the fact that we assume XX coupling to be equal to ZZ coupling. Furthermore, we only assume coupling between the target and directly connected spectators, omitting effects from all other couplings and environmental effects. These simplifications may, to some extent, explain mismatch with experimental data.

Another limitation is the inability of QuTiP's Bloch-Redfield solver to handle the $|+\rangle$ spectator configuration, likely due to numerical instability in the presence of off-diagonal coherence. This prevented us from testing whether Redfield dynamics could model the stabilization seen in that case. Future work should explore alternative non-Markovian solvers or perturbative approximations better suited to coherent bath states.

Finally, our data comes from a single three-qubit configuration on the IBM Sherbrooke device. To assess whether our results hold more generally, it would be important to replicate this protocol across multiple qubit layouts and hardware backends. Doing so would reveal whether the observed effects reflect universal trends or setup-specific idiosyncrasies.

4 Conclusion

We modeled crosstalk-induced decay on IBM Sherbrooke using the Lindblad and Bloch-Redfield equations and compared their predictions to experimental data under three spectator initializations: $|1\rangle$, $|0\rangle$, and $|+\rangle$. The Lindblad equation consistently underestimated late-time populations. The Bloch-Redfield equation matched early-time behavior more closely but decayed too quickly overall, remaining below experiment across the full window in the $|1\rangle$ and $|+\rangle$ cases.

The experimental data showed fastest decay with $|0\rangle$ spectators, consistent with enhanced dissipation through accessible relaxation pathways. Decay slowed significantly with $|1\rangle$ spectators due to Pauli blocking. The $|+\rangle$ case produced similar results to $|1\rangle$, suggesting that coherence in the spectator states suppresses energy transfer, an effect not captured by either model.

These results show that both equations miss essential features of spectator-induced decay. Neither handles coherent spectator states well, nor do they fully capture how state-dependent pathways shape relaxation. Modeling crosstalk in multi-qubit systems will require noise models that treat the environment as a quantum system, not just a weakly coupled bath.

5 Acknowledgments

We thank Daniel Lidar for helping us formulate the research idea, Juan Garcia Nila for guidance and feedback throughout the paper, and Kumar Saurav for providing valuable revisions and Arian Vezavee for helping guide us through the coupling extraction process.

References

[1] Rishabh Das, Ali Javadi-Abhari, Sarah Sheldon, Christopher J. Wood, and Jay M. Gambetta. Software mitigation of crosstalk on noisy intermediate-scale quantum computers, 2022. Technical report.

[2] Shashank Kumar and Manas Ramesh. Suppression of crosstalk in superconducting qubits using dynamical decoupling. ResearchGate Preprint, 2022.

[3] Daniel A. Lidar. Phys 550: Open quantum systems lecture notes, 2024. University of Southern California, Lecture Notes.

[4] Giacomo Torlai, Noah Ezzell, Juan Carrasquilla, Nathan Wiebe, and Man-Hong Yung. Non-markovian process characterization via classical shadows. *arXiv preprint arXiv:2403.09944*, 2024.